Draft version April 13, 2023
Typeset using LaTeX **twocolumn** style in AASTeX631

The interstellar medium in host galaxies of the brightest $z > 6$ radio-loud quasars

Y. Khusanova[1] and et al.[2]

[1] *Max-Planck-Institut für Astronomie, Königstuhl 17, D-69117 Heidelberg, Germany*
[2] *XX*

ABSTRACT

The interstellar medium (ISM) in galaxies with active galactic nuclei (AGN) is affected by both star formation and black hole activity. In radio-loud quasars, the ISM can be additionally affected by relativistic jets. The quasar host galaxies at the highest redshifts are laboratories to explore the conditions of the ISM in galaxies with rapidly growing black holes. Molecular and atomic emission line provide diagnostic tools to investigate the properties of the ISM and the main sources of gas heating and excitation. We present CO(6-5), CO(7-6), [CI] and underlying continuum observations in two radio-loud quasars at $z > 6$ which are the brightest in FIR, X-ray, radio and [CII] emission. We detect all targeted emission lines and continuum in both systems. We show that despite very similar properties across wavelength range, the ISM properties are different. In J1429+5447, the gas has moderate density and is heated mainly by star formation. On the other hand, J0309+2717 contains higher density gas heated by strong X-ray radiation from the AGN. Our results show that the conditions in the ISM are not solely defined by the AGN properties and star formation rate in the host galaxy.

1. INTRODUCTION

The role of different mechanisms regulating star formation in a galaxy is poorly understood. Observations show that some galaxies have their star formation quenched already at $z = 4$ (e.g., Forrest et al. 2020). JWST pushed this redshift limit even further: numberous quiescent galaxies were discovered at $3 < z < 5$ (Carnall et al. 2023), and even at $z = 7.3$ (Looser et al. 2023). Explaining such rapid shut-down of star formation is challenging for theoretical models. Active Galactic Nuclei (AGN) feedback is thought to play an important role in regulating star formation (Man & Belli 2018). Negative AGN feedback prevents star formation by heating the gas or removing the gas via AGN-driven outflows (e.g., Di Matteo et al. 2005; Villar Martín et al. 2014). Positive AGN feedback can enhance star formation via AGN-induced pressure (Silk 2013). Numerous observations of quasar host galaxies have been carried out to investigate whether AGN could be responsible for the negative feedback. However, only recently observations of radio-loud quasar host galaxies at $z > 5.8$ became available (Rojas-Ruiz et al. 2021; Khusanova et al. 2022).

Radio-loud quasars are defined as quasars with radio-loudness $R_{4400} > 10$[1]. Such high radio to optical emission ratio is cause by a presence of a jet. Simulations show that the jet can cause negative feedback as well as positive feedback on the star formation (Mandal et al. 2021), depending on the jet orientation and age. This is yet to be confirmed with observations. Khusanova et al. (2022) give hints that the jets can cause negative feedback based on measurements of the star formation rate (SFR) in their host galaxies. Using [CII] emission and FIR continuum flux density is not trivial in case of radio-loud quasars. Rojas et al. 2022 show that the FIR flux of radio-loud quasars can be contaminated by the synchrotron emission of the jet. Therefore, SFR measured using the rest-frame FIR continuum flux can be overestimated. The [CII] emission has been proven to be a good star formation tracer in main sequence galaxies (De Looze et al. 2014; Schaerer et al. 2020) as well as radio-quiet quasar host galaxies (Venemans et al. 2017; Pensabene et al. 2021; Decarli et al. 2022; Meyer et al. 2022), since it is mainly originating from PDR in those cases. However, [CII] emission can also be produced by gas excited by strong X-ray radiation from AGN. An-

[1] $R_{4400} = S_{5GHz}/S_{4400}$, where S_{5GHz} and S_{4400} are flux densities at the rest-frame at 5 GHz and 4400 Å, respectively (Kellermann et al. 1989).

other way to produce [CII] emission is through shocks, which might be common among radio-loud AGN, since shocks can be due to propagation of the jet in ISM. Therefore, a careful analysis of the origin of the [CII] and FIR emission in radio-loud quasar hosts is necessary.

Most radio-loud quasars at $z > 5.8$, which have been observed at mm wavelength, are hosted in galaxies with moderate or low SFRs (below the median of the SFR distribution of radio-quiet quasar hosts at same redshifts, Khusanova et al. 2022). Only two (J1429 and J0309) have distinctly high [CII] and IR luminosities. They are the most radio-loud sources at $z > 6$ (Bañados et al. 2015; Belladitta et al. 2020). J1429 is the brightest X-ray source at $z > 6$ (Medvedev et al. 2020, 2021) followed by J0309 (Belladitta et al. 2020), which means that XDR may play an important role in [CII] emission origin. Besides, Wang et al. (2011) have observed CO(2–1) emission from J1429 and show tentatively a presence of the second component, only detected at CO(2–1) wavelength with 4σ significance. Similarly, the [CII] emission profile of J1429 can be divided into two Gaussian components with similar line widths (Khusanova et al. 2022). These observations suggest that the host galaxy of J1429 may be a merger and [CII] emission can be produced via shocks.

In order to obtain robust SFR measurements of J1429 and J0309, we observed their [CI], CO(7–6) and CO(6–5) emission and underlying continuum with NOEMA. Here we present our results and analysis of the origin of the [CII] emission and the fraction of synchrotron contribution to the FIR continuum flux densities. The paper is organized as follows. XX. Throughout the paper, we use cosmology with XX.

2. DATA

The [CII] and FIR brightest radio-loud quasars J1429 and J0309 were observed with NOEMA in band 1 in July and August, 2021 (program number S21DG). The total on source time was 12.5 and 16.1 hours for J1429 and J0309 respectively. Observations were done with 10 antennae.We followed standard calibration steps using the Grenoble Image and Line Data Analysis Software (GILDAS)[2]. In Table 1, we provide a summary of all observations and calibration sources used. In the end, we produced two data cubes for each source corresponding to upper and lower side bands (USB and LSB). The USB covers frequencies from 91.4 to 99.1 GHz and the LSB covers frequencies from 106.9 to 114.6 GHz.

[2] https://www.iram.fr/IRAMFR/GILDAS

First, we extract spectra from the optical position of the quasar. We search for CO(7–6) and [CI] in the USB, and CO(6–5) in the LSB. In both J1429 and J0309, we find all emission lines at their expected positions based on redshift measured via [CII] emission. We fit all the lines with a single Gaussian. We produce LSB and USB continuum images by averaging all the channels in the cubes except for ± 1000 km s^{-1} from the line centers. In order to produce line images, we first subtract the continuum from the whole cube by using UV_BASELINE and excluding channels containing lines as described above. After continuum subtraction, we extract line images by averaging channels in 1.2 FWHM range.

3. RESULTS

We show the images and spectra of J1429 and J0309 in Fig. 1 and 2 respectively. In Table 2, we present FWHM, line and continuum luminosity measurements.

3.1. *Continuum*

We show SED of our targets in Fig. 3. We find that continuum flux densities of J0309+2717 cannot be explained solely by the modified black body (MBB) model as they are contaminated by the synchrotron emission from the jet. Mufakharov et al. (2020) observations of J0309+2717 with RATAN-600 suggest that the slope of J0309+2717 radio emission significantly steepens at frequencies higher than 10 GHz. This would mean negligible contribution from synchrotron emission to ~ 100 GHz flux densities, which is in disagreement with our data. However, our flux density measurements agree well with the power law extrapolated from the VLA observations at XX-XX GHz (Spingola et al. 2020).

J1429+5447 was previously observed with NOEMA at XX to XX GHz (Li et al. XX). The find a good agreement between our flux density measurements and measurements in (Li et al. XX) except for 97 GHz measurement. Our 97 GHz continuum measurement is 2.7 times higher than in Li et al. XX. We note that 98 GHz flux density in Li et al. XX is significantly lower than any other continuum flux densities at 82-112 GHz. These frequencies are also more affected by the synchrotron emission. Possible variability of the synchrotron emission can affect the measurements and requires further investigation.

3.2. *Emission lines*

We find all three emission lines (CO(6-5), CO(7-6), [CI]) in the spectra of both J0309+2717 and J1429+5447. The widths of the lines of J0309+2717 are in agreement with each other as well as with [CII]

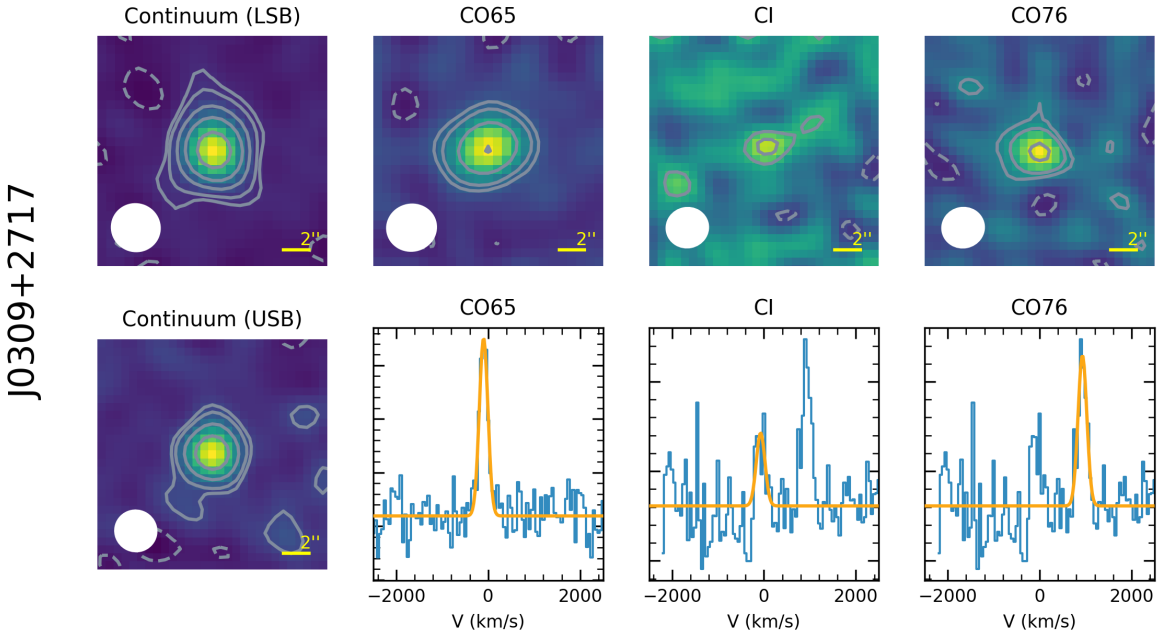

Figure 1. First column: the continuum images of J0309+2717. Second column: the CO(6–5) line image and spectral profile. The orange line is the best fit with a Gaussian. Third column: the [CI] line image and spectral profile. Forth column: the CO(7–6) line image.

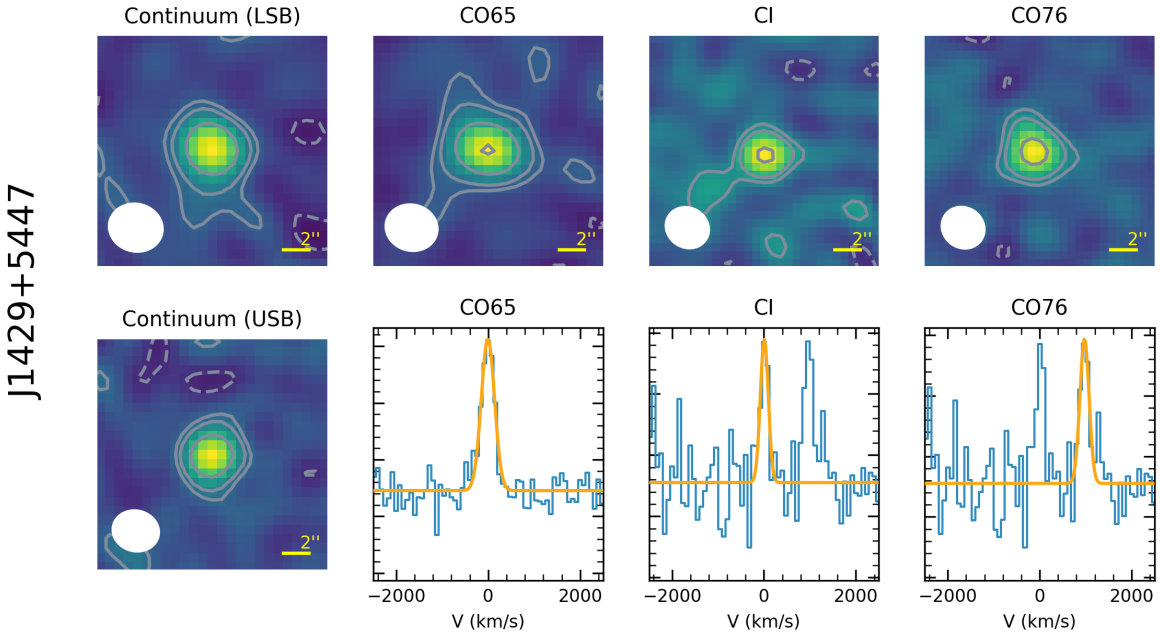

Figure 2. Same as 1 but for J1429+5447

Source	Date	On source time	Number of antennas	Bandpass	Phase and amplitude	Flux density
J1429+5447	17-jun-2021	1.9	10	3C345	1418+546	MWC349
	04-jul-2021	1.9	10	3C273	1418+546	MWC349
	28-jul-2021	1.5	10	3C273	1418+546	MWC349
	01-aug-2021	4.2	10	3C84	1418+546	LKHA101
	05-aug-2021	1.9	10	3C273	1418+546	MWC349
	09-aug-2021	1.1	10	1741-038	1418+546	MWC349
J0309+2717	17-jun-2021	4.2	10	2013+370	0234+285	MWC349
	01-jul-2021	3.4	10	3C454.3	0234+285	MWC349
	02-jul-2021	5.2	10	3C454.3	0234+285	MWC349
	14-jul-2021	1.1	10	3C84	0234+285	LKHA101
	17-jul-2021	2.2	10	3C454.3	0234+285	MWC349

Table 1. A summary of observations and calibrators used in data reduction.

	J0309+2717			J1429+5447		
Line	FWHM	Flux (Jy km s^{-1})	L ($\times 10^8 L_\odot$)	FWHM	Flux (Jy km s^{-1})	L ($\times 10^8 L_\odot$)
CO(6-5)	220 ± 18	0.30 ± 0.02	1.05 ± 0.07	340 ± 30	0.26 ± 0.03	0.93 ± 0.10
CO(7-6)	225 ± 31	0.30 ± 0.03	1.23 ± 0.13	234 ± 55	0.26 ± 0.04	1.08 ± 0.13
CI	223 ± 64	0.14 ± 0.03	0.57 ± 0.12	204 ± 52	0.20 ± 0.03	0.84 ± 0.13
Freq		Flux (mJy)	L ($\times 10^{12} L_\odot$)		Flux (mJy)	L ($\times 10^{12} L_\odot$)
93.2		0.56 ± 0.02			0.21 ± 0.02	
97.3		0.58 ± 0.03			0.24 ± 0.02	
108.7		0.65 ± 0.03			0.24 ± 0.02	
112.8		0.67 ± 0.04			0.29 ± 0.04	

Table 2. Emission line and underlying continuum flux measurements.

emission line within the error bars (Khusanova et al. 2022). The width CO(6-5) emission line of J1429+5447 is consistent with the width of [CII] line fit with a single Gaussian. The widths of CO(7-6) and [CI] are significantly narrow but are consistent with the width of the narrow component in [CII] and CO(2-1) emission lines (Wang et al. 2011; Khusanova et al. 2022). The CO(7-6) and [CI] can, therefore, be coming from the same region as the narrow component of [CII] emission line, while CO(6-5), CO(2-1) and [CII] emission from both narrow and broad line components.

4. DISCUSSION

4.1. *The dust properties*

Continuum flux density measurements allow us to simultaneously fit the MBB model of cold dust emission and power law model of synchrotron emission in radio. We show the results in Fig. 3. We find significantly higher dust temperatures than typically assumed $T_{dust} = 47$ K. The dust temperatures are 83^{+35}_{-20} K and 60^{+11}_{-7} for J0309+2717 and J1429+5447 respectively. Such high dust temperatures could be caused by heating by AGN (Di Mascia et al. 2023). In that case, SFRs estimated using IR luminosity would be overestimated.

Continuum flux densities of J1429+5447 can be fit with MBB without adding contribution from the synchrotron. The spectral slope of synchrotron emission can steepen in young jets (Rojas-Ruiz et al. 2021). If this is the case for J1429+5447, the contribution of the synchrotron emission would be negligible. We, therefore, consider two cases: with and without contribution from the synchrotron emission.

4.2. *The ISM properties*

In quasar host galaxies both AGN and star formation play a role in exciting and heating gas in the ISM. However, according to multi-line studies of radio-quiet quasars, [CII] line emission originates from PDR, and XDR contribution is negligible (Venemans et al. 2017; **?**; Pensabene et al. 2021; Meyer et al. 2022; Decarli et al. 2022). However, no such study has been done on the host galaxies of radio-loud quasars. The [CII] brightest radio-loud quasars at $z > 6$ are also the brightest X-ray sources. Hence, the effect of XDR on the ISM is potentially stronger than in radio-quiet quasars.

We measure line flux ratios of J0309+2717 and J1429+5447, and use the XDR and PDR models from Pensabene et al. (2021) to calculate line flux ratios for different column densities and radiation field intensities. XDR models have low [CII]/[CI] ratio compared to PDR models. Li et al. XX observed [CI] emission line of J1429+5447 but it was non-detect. Here, we for the first time detect [CI] emission line in two radio-loud quasars. We find $[CII]/[CI] = 44$ and $[CII]/[CI] = 98$ for J0309+2717 and J1429+5447 respectively.

The $[CII]/[CI]$ is significantly low in case of J1429+5447 and does not agree neither with PDR nor with XDR models. One reason for such low $[CII]/[CI]$ ratio is significantly broader FWHM of the [CII] line. Assuming the same width for [CI] line as the width of [CII] line, we find $[CII]/[CI] = 55$ and use as a lower limit for the $[CII]/[CI] = 55$ ratio. We show the line ratios in Fig. 4. Only for the lowest values of $[CII]/[CI]$, we find an agreement between the ratios. In case of moderate column density $N_H = 10^{23}$ cm^{-2}, we find an agreement for hydrogen density $n_H = 10^{4-6}$ cm^{-3} and incident radiation $G_0 = 10^{4-4.6}$. In case of low column density $N_H = 10^{23}$ cm^{-2}, we find values $n_H = 10^{2.5-6.0}$ cm^{-3} and incident radiation $G_0 = 10^{3.2-4.5}$. None of XDR models agrees with high $[CII]/[CI]$ ratio found in J1429+5447.

Although we considered the same [CII] and [CI] line width, we note that previous observations of J1429+5447 showed two components of CO(2–1) emission (Wang et al. 2011) indicative of a merger. The [CII] emission line also has two components according to the fit of the line profile with two Gaussians (Khusanova et al. 2022). Observed [CI] width is in good agreement with the narrow component. Hence, the observed [CI] emission can originate from the narrow component while [CII] line luminosity contains both components. Currently available [CII] and [CI] images have insufficient spatial resolution to disentangle the two components. Therefore, the results should be interpreted with a caution.

The ratios of [CII] and CO lines agree across wide range of hydrogen densities and radiation field strength for J1429+5447 for moderate column density $N_H = 10^{23}$ cm^{-2}. For low column densities, they require low radiation field and high hydrogen density, and for high column density, both incident radiation and hydrogen density should be high. As in case of atomic lines luminosity ratios, no XDR model can explain luminosity ratios with CO lines. We find that both atomic and molecular line ratios are best explained by PDR models for column density $N_H = 10^{23}$ cm^{-2}, hydrogen density $n_H = 10^{4-6}$ cm^{-3} and incident radiation $G_0 = 10^{4-4.6}$ in J1429+5447.

Our results indicate PDR origin of gas excitation. However, Li et al. XX show that luminosity ratios and low excitation of higher CO transitions ($J_{upper} = 9, 10$) can be explained by a combination of XDR and PDR models ($n_H = 10^{3.4^{+1.1}_{-1.0}}$ cm^{-3} and $G_0 = 10^{3.8\pm0.8}$ for

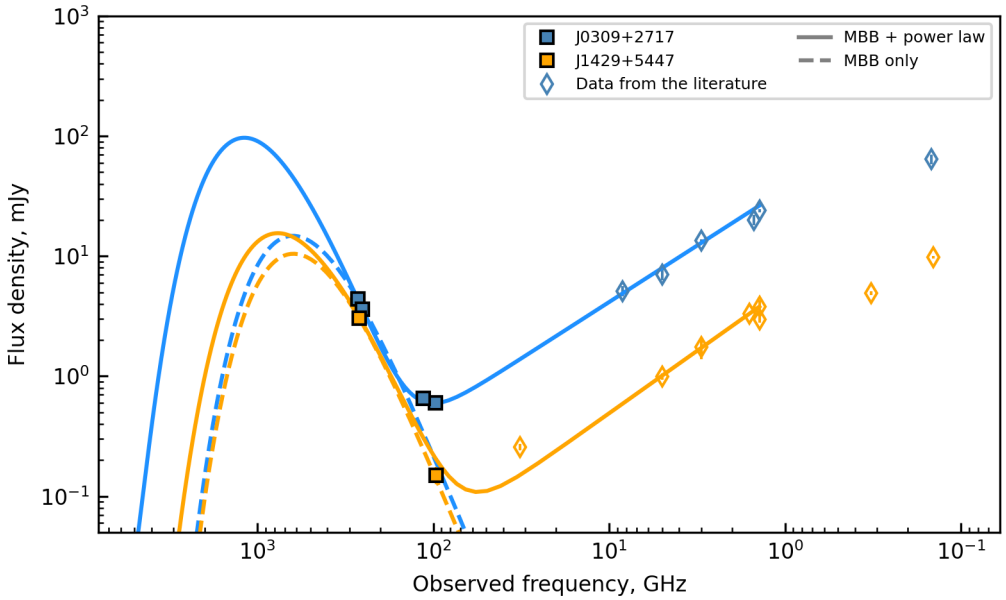

Figure 3. SEDs of J0309 and J1429. The filled symbols are measurements of the continuum flux density (NOEMA measurements presented in this paper and literature data at 250 GHz Khusanova et al. 2022). The orange and blue solid lines are a sum of MBB model and a power law fit to the continuum flux densities of J1429+5447 and J0309+2717 respectively. The dashed lines are MBB models scaled to NOEMA flux density measurements at 250 GHz. The literature data (Bañados et al. 2021; Condon et al. 1998; Frey et al. 2008, 2011; Ighina et al. 2021; Intema et al. 2017; Momjian et al. 2008; Shimwell et al. 2019; Wang et al. 2011) are shown with thin diamonds.

PDR model, $n_H = 10^{5.8^{+0.7}_{-0.3}}$ cm^{-3} and $F_X = 10^{1.6^{+0.9}_{-1.1}}$ erg s^{-1} cm^{-1} for XDR model).

In the case of J0309+2717, we find that for high and moderate column densities, the radiation field is high ($G_0 > 10^{4.3}$). The hydrogen density is $n_H = 10^{3.9-6}$ cm^{-3} and $n_H = 10^{3.1-6.0}$ cm^{-3}, for high and moderate column density respectively. Low column density models agree well with $G_0 = 10^{3.5-4.3}$ and low hydrogen density $n_H < 10^{2.7}$ cm^{-3}. The XDR models agree with luminosity ratios observed in J0309+2717 only in case of strong radiation field $F_X = 10^{0.8-2}$ erg s^{-1} cm^{-1} and for the whole range of hydrogen density considered.

The luminosity ratios with molecular lines only agree for high column density in the case of PDR models for J0309+2717, and with low column density in case of XDR models. However, high column density models do not explain the luminosity ratios with atomic lines. Only XDR model with low column density $N_H = 10^{22}$ cm^{-2}, hydrogen density $n_H = 10^{4.7-5.0}$ cm^{-3} and strong incident radiation $F_X = 10^{1.5-2.0}$ erg s^{-1} cm^{-1} can explain the luminosity line ratios in J0309+2717.

Higher CO transitions have not yet been observed for J0309+2717, however, the properties of J0309+2717 are similar to J215.15, a radio-quiet quasar at $z = 5.78$. The CO SLED of J215.15 shows high excitation powered by strong X-ray radiation from the AGN and high gas density (Li et al. XX). J1429+5447 is, on the other hand, has low CO excitation and moderate gas density. The moderate gas density could be explained by the presence of the jet removing gas from the host galaxy. However, in that case, J0309+2717 should have moderate gas density as well, which is not consistent with CO luminosity ratios of J0309+2717. The differences in ISM properties of J1429+5447 and J215.15, therefore, cannot be explained by radio-loudness of J1429+5447.

5. CONCLUSIONS

We observed [CI], CO(6-5) and CO(7–6) emission lines and underlying continuum in the brightest radio-loud quasars at $z > 6$. The ISM properties of J1429+5447 are best explained by PDR models. However, $[CII]/[CI]$ ratio is inconsistent with the models if the widths difference of [CII] and [CI] lines is real. Possible presence of a second component of [CII] emission can be a reason for inconsistency of $[CII]/[CI]$ ratio with models.

J0309+2717 shows signs of AGN contribution to CO excitation and gas heating. Only XDR models can explain luminosity ratios observed in J0309+2717. The difference between properties of J0309+2717 and J1429+5447, the only two radio-loud quasars with observed CO emission lines, means that complex processes affect ISM in quasar host galaxy and presence of a jet cannot explain previously reported difference between radio-quiet and radio-loud quasars.

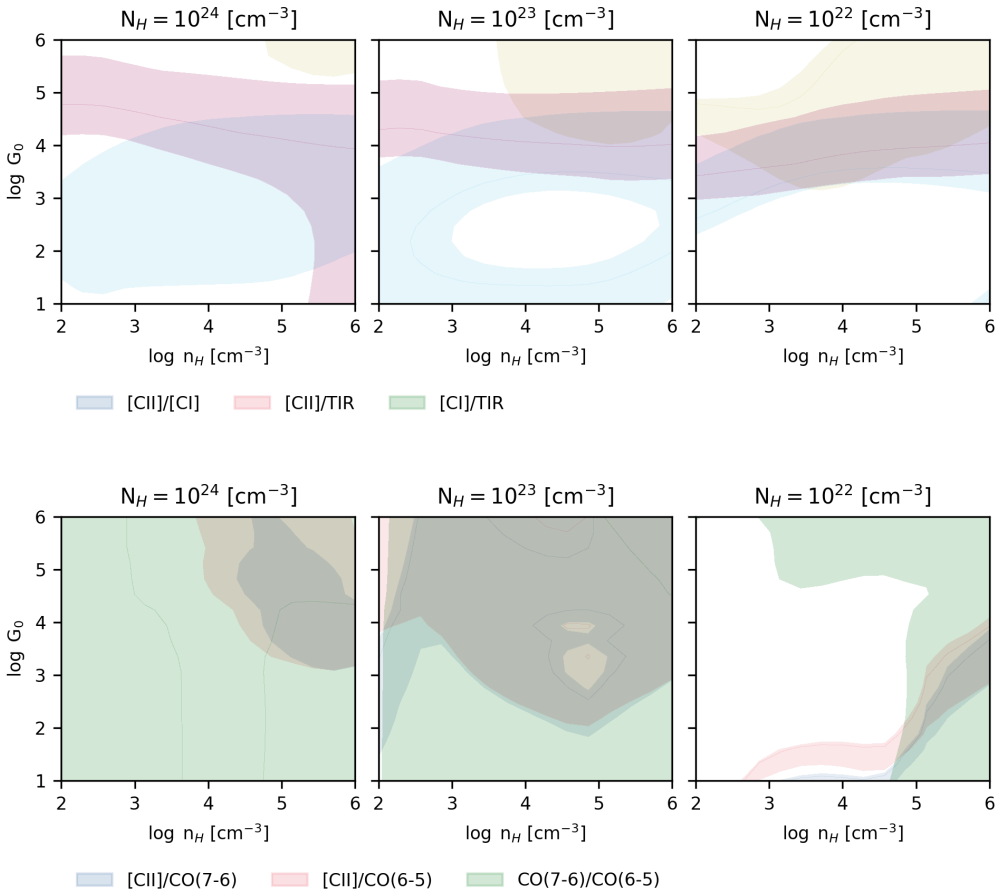

Figure 4. PDR model predictions of line ratios. The shaded areas show the corresponding line ratios measured in J1429.

Based on observations carried out under project number S21DG with the IRAM NOEMA Interferometer. IRAM is supported by INSU/CNRS (France), MPG (Germany) and IGN (Spain). Y.K. thanks the IRAM staff for help provided during the observations and for data reduction.

Facilities: NOEMA

Software: astropy (**??**), GILDAS

REFERENCES

Bañados, E., Venemans, B. P., Morganson, E., et al. 2015, ApJ, 804, 118, doi: 10.1088/0004-637X/804/2/118

Bañados, E., Mazzucchelli, C., Momjian, E., et al. 2021, ApJ, 909, 80, doi: 10.3847/1538-4357/abe239

Belladitta, S., Moretti, A., Caccianiga, A., et al. 2020, A&A, 635, L7, doi: 10.1051/0004-6361/201937395

Carnall, A. C., McLeod, D. J., McLure, R. J., et al. 2023, MNRAS, doi: 10.1093/mnras/stad369

Condon, J. J., Cotton, W. D., Greisen, E. W., et al. 1998, AJ, 115, 1693, doi: 10.1086/300337

De Looze, I., Cormier, D., Lebouteiller, V., et al. 2014, A&A, 568, A62, doi: 10.1051/0004-6361/201322489

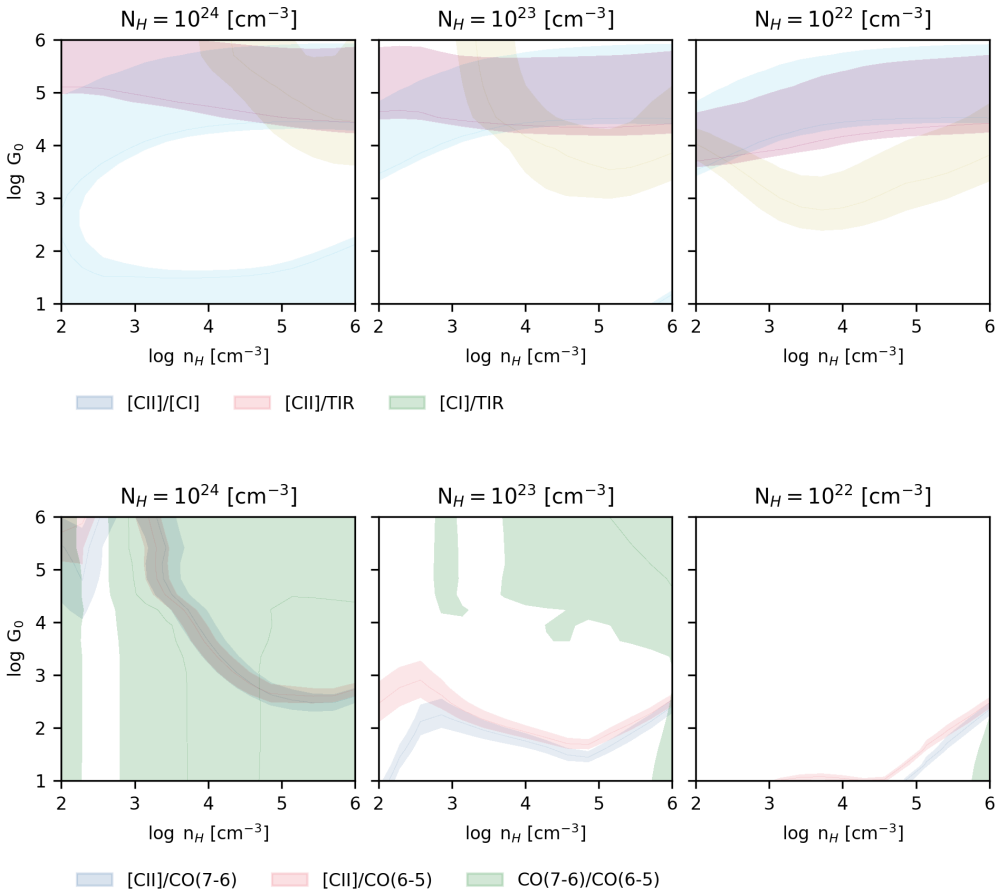

Figure 5. Same as Fig. 4 but for J0309.

Decarli, R., Pensabene, A., Venemans, B., et al. 2022, A&A, 662, A60, doi: 10.1051/0004-6361/202142871

Di Mascia, F., Carniani, S., Gallerani, S., et al. 2023, MNRAS, 518, 3667, doi: 10.1093/mnras/stac3306

Di Matteo, T., Springel, V., & Hernquist, L. 2005, Nature, 433, 604, doi: 10.1038/nature03335

Forrest, B., Annunziatella, M., Wilson, G., et al. 2020, ApJL, 890, L1, doi: 10.3847/2041-8213/ab5b9f

Frey, S., Gurvits, L. I., Paragi, Z., & É. Gabányi, K. 2008, A&A, 484, L39, doi: 10.1051/0004-6361:200810040

Frey, S., Paragi, Z., Gurvits, L. I., Gabányi, K. É., & Cseh, D. 2011, A&A, 531, L5, doi: 10.1051/0004-6361/201117341

Ighina, L., Belladitta, S., Caccianiga, A., et al. 2021, arXiv e-prints, arXiv:2101.11371. https://arxiv.org/abs/2101.11371

Intema, H. T., Jagannathan, P., Mooley, K. P., & Frail, D. A. 2017, A&A, 598, A78, doi: 10.1051/0004-6361/201628536

Kellermann, K. I., Sramek, R., Schmidt, M., Shaffer, D. B., & Green, R. 1989, AJ, 98, 1195, doi: 10.1086/115207

Khusanova, Y., Bañados, E., Mazzucchelli, C., et al. 2022, A&A, 664, A39, doi: 10.1051/0004-6361/202243660

Looser, T. J., D'Eugenio, F., Maiolino, R., et al. 2023, arXiv e-prints, arXiv:2302.14155, doi: 10.48550/arXiv.2302.14155

Man, A., & Belli, S. 2018, Nature Astronomy, 2, 695, doi: 10.1038/s41550-018-0558-1

Mandal, A., Mukherjee, D., Federrath, C., et al. 2021, MNRAS, doi: 10.1093/mnras/stab2822

Medvedev, P., Gilfanov, M., Sazonov, S., Schartel, N., & Sunyaev, R. 2021, MNRAS, 504, 576, doi: 10.1093/mnras/stab773

Medvedev, P., Sazonov, S., Gilfanov, M., et al. 2020, MNRAS, 497, 1842, doi: 10.1093/mnras/staa2051

Meyer, R. A., Walter, F., Cicone, C., et al. 2022, arXiv e-prints, arXiv:2201.08143. https://arxiv.org/abs/2201.08143

Momjian, E., Carilli, C. L., & McGreer, I. D. 2008, AJ, 136, 344, doi: 10.1088/0004-6256/136/1/344

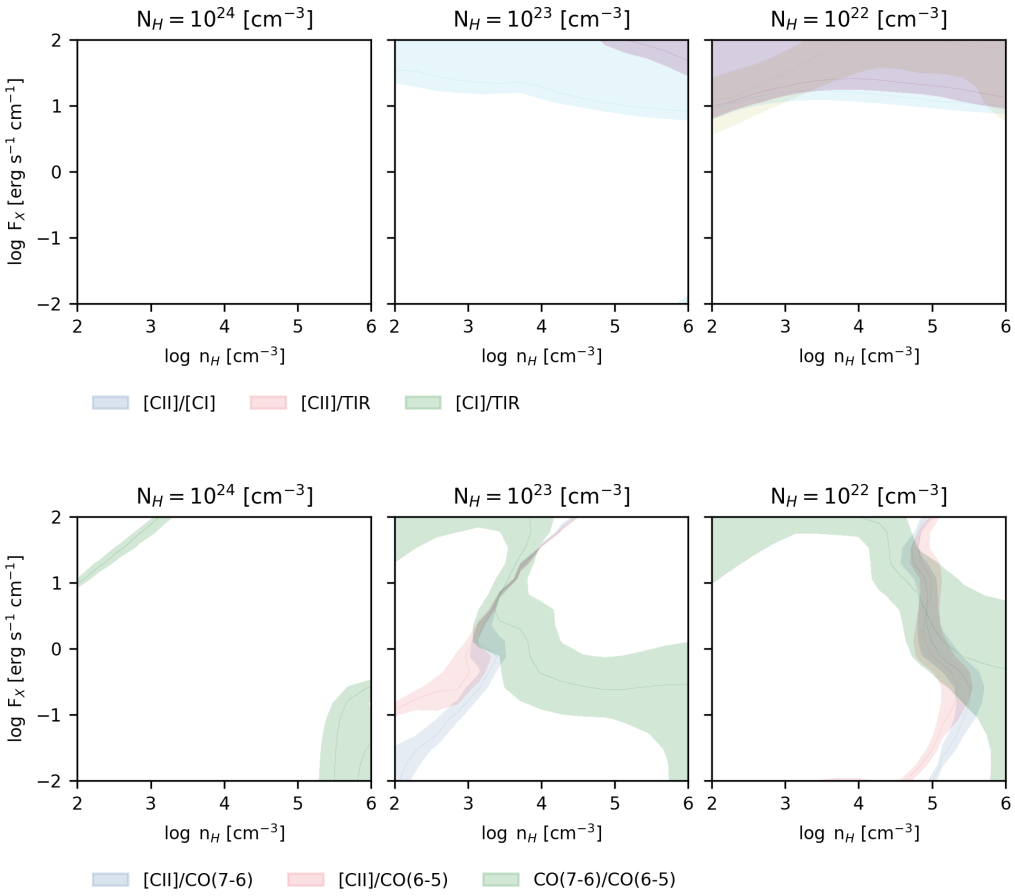

Figure 6. Same as Fig. 5 but for XDR models.

Mufakharov, T., Mikhailov, A., Sotnikova, Y., et al. 2020, arXiv e-prints, arXiv:2011.12072. https://arxiv.org/abs/2011.12072

Pensabene, A., Decarli, R., Bañados, E., et al. 2021, A&A, 652, A66, doi: 10.1051/0004-6361/202039696

Rojas-Ruiz, S., Bañados, E., Neeleman, M., et al. 2021, ApJ, 920, 150, doi: 10.3847/1538-4357/ac1a13

Schaerer, D., Ginolfi, M., Béthermin, M., et al. 2020, A&A, 643, A3, doi: 10.1051/0004-6361/202037617

Shimwell, T. W., Tasse, C., Hardcastle, M. J., et al. 2019, A&A, 622, A1, doi: 10.1051/0004-6361/201833559

Silk, J. 2013, ApJ, 772, 112, doi: 10.1088/0004-637X/772/2/112

Spingola, C., Dallacasa, D., Belladitta, S., et al. 2020, A&A, 643, L12, doi: 10.1051/0004-6361/202039458

Venemans, B. P., Walter, F., Decarli, R., et al. 2017, ApJL, 851, L8, doi: 10.3847/2041-8213/aa943a

Villar Martín, M., Emonts, B., Humphrey, A., Cabrera Lavers, A., & Binette, L. 2014, MNRAS, 440, 3202, doi: 10.1093/mnras/stu448

Wang, R., Wagg, J., Carilli, C. L., et al. 2011, ApJL, 739, L34, doi: 10.1088/2041-8205/739/1/L34